BJP British Journal of Pharmacology

DOI:10.1111/bph.13022
www.brjpharmacol.org

Themed Section: Annexins VII Programme

RESEARCH PAPER

Evidence for annexin A6-dependent plasma membrane remodelling of lipid domains

Anna Alvarez-Guaita[1]*, Sandra Vilà de Muga[1]*, Dylan M Owen[2†], David Williamson[2‡], Astrid Magenau[2§], Ana García-Melero[1], Meritxell Reverter[1], Monira Hoque[3], Rose Cairns[3], Rhea Cornely[2], Francesc Tebar[1], Thomas Grewal[3], Katharina Gaus[2], Jesús Ayala-Sanmartín[4], Carlos Enrich[1,5] and Carles Rentero[1]

[1]*Departament de Biologia Cel·lular, Immunologia i Neurociències, Facultat de Medicina, Universitat de Barcelona, Barcelona, Spain,* [2]*Center for Vascular Research, The University of New South Wales, Sydney, NSW, Australia,* [3]*Faculty of Pharmacy, University of Sydney, Sydney, NSW, Australia,* [4]*Centre National de la Recherche Scientifique (CNRS), École Normale Supérieure (ENS) and Université Pierre et Marie Curie (UPMC), Paris, France, and* [5]*Centre de Recerca Biomèdica CELLEX, Institut d'Investigacions Biomèdiques August Pi i Sunyer (IDIBAPS), Barcelona, Spain*

Correspondence
Carles Rentero and Carlos Enrich, Departament de Biologia Cel·lular, Immunologia i Neurociències, Facultat de Medicina, Universitat de Barcelona, 08036 Barcelona, Spain. E-mail: carles.rentero@ub.edu; enrich@ub.edu

*Both authors contributed equally.

Present addresses: †Department of Physics and Randall Division of Cell and Molecular Biophysics, King's College London, London WC2R 2LS, UK.

‡Faculty of Life Sciences, University of Manchester, Manchester M13 9PT, UK.

§Garvan Institute of Medical Research and Kinghorn Cancer Centre, Cancer Research Program, St. Vincent's Clinical School, Faculty of Medicine, University of New South Wales, Sydney, NSW 2010, Australia.

Received
2 April 2014
Revised
11 November 2014
Accepted
14 November 2014

BACKGROUND AND PURPOSE

Annexin A6 (AnxA6) is a calcium-dependent phospholipid-binding protein that can be recruited to the plasma membrane to function as a scaffolding protein to regulate signal complex formation, endo- and exocytic pathways as well as distribution of cellular cholesterol. Here, we have investigated how AnxA6 influences the membrane order.

EXPERIMENTAL APPROACH

We used Laurdan and di-4-ANEPPDHQ staining in (i) artificial membranes; (ii) live cells to investigate membrane packing and ordered lipid phases; and (iii) a super-resolution imaging (photoactivated localization microscopy, PALM) and Ripley's K second-order point pattern analysis approach to assess how AnxA6 regulates plasma membrane order domains and protein clustering.

KEY RESULTS

In artificial membranes, purified AnxA6 induced a global increase in membrane order. However, confocal microscopy using di-4-ANEPPDHQ in live cells showed that cells expressing AnxA6, which reduces plasma membrane cholesterol levels and modifies the actin cytoskeleton meshwork, displayed a decrease in membrane order (~15 and 30% in A431 and MEF cells respectively). PALM data from Lck10 and Src15 membrane raft/non-raft markers revealed that AnxA6 expression induced clustering of both raft and non-raft markers. Altered clustering of Lck10 and Src15 in cells expressing AnxA6 was also observed after cholesterol extraction with methyl-β-cyclodextrin or actin cytoskeleton disruption with latrunculin B.

© 2014 The British Pharmacological Society

CONCLUSIONS AND IMPLICATIONS

AnxA6-induced plasma membrane remodelling indicated that elevated AnxA6 expression decreased membrane order through the regulation of cellular cholesterol homeostasis and the actin cytoskeleton. This study provides the first evidence from live cells that support current models of annexins as membrane organizers.

LINKED ARTICLES

This article is part of a themed section on Annexins VII Programme. To view the other articles in this section visit http://dx.doi.org/10.1111/bph.2015.172.issue-7

Abbreviations

A6ko, annexin A6 knockout; AnxA1, annexin A1; AnxA2, annexin A2; AnxA6, annexin A6; $cPLA_2$, cytoplasmic phospholipase A_2; DRM, detergent-resistant membrane; EGFR, epidermal growth factor receptor; Lat34, transmembrane domain of linker for activation of T-cells; LatB, latrunculin B; Laurdan, 6-dodecanoyl-2-dimethylaminonaphthalene; Lck10, 10 first amino acids of Lck; Ld, liquid-disordered domain; Lo, liquid-ordered domain; LUV, large unilamellar vesicle; mβCD, methyl-β-cyclodextrin; MEF, mouse embryonic fibroblast; PALM, photoactivated localization microscopy; PC, phosphatidylcholine; PE, phosphatidylethanolamine; PFA, paraformaldehyde; PIP_2, phosphatidylinositol-4,5-bisphosphate; PS, phosphatidylserine; *r*, radius; Src15, 15 first amino acids of Src; TIRF, total internal reflection fluorescence; WT, wild type

Tables of Links

TARGETS
Enzymes[a]
Phospholipase A_2
PKCα
Catalytic receptor[b]
EGFR, EGF receptor

LIGANDS
AnxA1, annexin A1
Cholesterol
PE, phosphatidylethanolamine
PIP_2, phosphatidylinositol-4,5-bisphosphate
PS, phosphatidyl-L-serine

These Tables list key protein targets and ligands in this article which are hyperlinked to corresponding entries in http://www.guidetopharmacology.org, the common portal for data from the IUPHAR/BPS Guide to PHARMACOLOGY (Pawson *et al.*, 2014) and are permanently archived in the Concise Guide to PHARMACOLOGY 2013/14 ([a,b]Alexander *et al.*, 2013a,b).

Introduction

The cellular plasma membrane was initially described as a two-dimensional homogeneous fluid cell compartment in which lipids and embedded proteins are able to diffuse in the lateral dimension (Singer and Nicolson, 1972; Nicolson, 2014). The plasma membrane sets a physical barrier and selectively regulates the molecules that pass through, delimiting an intra- and an extracellular space. This selective permeability is critical for drug diffusion into the cell (Sugano *et al.*, 2010).

Following many observations showing that proteins are not homogeneously distributed in the plasma membrane, Simons and Ikonen (1997) proposed the lipid raft hypothesis. In this model, lipids not only play a structural role but mediate protein clustering and diffusion parameters within the bilayer inducing lateral heterogeneity of proteins and lipids. It postulates the existence of cholesterol- and sphingolipid-enriched, ordered-phase liquid (Lo) domains surrounded by the bulk liquid-disordered (Ld) membrane. These domains create lateral heterogeneity and functionality as highly efficient transient platforms for clustering of specific proteins in cell membranes (Parton and Richards, 2003). Many of these raft clustered proteins function in cell signalling and endocytosis, as described for immune and other cell types (Simons and Toomre, 2000; Jacobson *et al.*, 2007). Membrane cholesterol concentration has also been described as a regulator of membrane permeability of both hydrophilic and hydrophobic solutes by changing the phospholipid packing conformation of the lipid bilayer affecting drug delivery (Zocher *et al.*, 2013).

New findings have prompted researchers to revisit and update the lipid raft hypothesis in the last few years. Kusumi and colleagues proposed that the cortical actin meshwork, together with lipid rafts and membrane proteins, regulates lateral diffusion of plasma membrane components (Ritchie *et al.*, 2003; Kusumi *et al.*, 2004). A transient tethering of the cortical actin filaments (fences) with transmembrane proteins (pickets) would divide the plasma membrane in corrals, which would orchestrate protein and lipid lateral diffusion and, among others, contribute to several cellular processes such as cell migration, mechanotransduction and immune cell activation (Head *et al.*, 2014). Other studies identified actin-associated 'protein islands' in the plasma membrane surrounded by protein-free membrane characterized by very low amounts of cholesterol. In contrast, the 'protein islands' can have high (raft) or low (non-raft) cholesterol content (Lillemeier *et al.*, 2006). Targeting fluorescent proteins to different domains of the plasma membrane, for instance, Lck10 (first 10 amino acids of Lck) and

transmembrane domain of linker for activation of T-cells (Lat34) to lipid rafts, and Src15 (first 15 residues of Src) to non-lipid rafts, allowed the definition of the role of the actin cytoskeleton in inducing co-clustering of raft-associated proteins by FRET microscopy (Chichili and Rodgers, 2007). Strikingly, actin promotes protein clustering and regulates the protein phosphorylation of raft-associated signalling proteins. More recent findings suggest that the actin meshwork can induce membrane partitioning with Lo-enriched compartments surrounded by Ld-enriched domains that correlate with the actin fibres (Honigmann *et al.*, 2014).

Adding further complexity, plasma membrane cholesterol/membrane rafts can also regulate the cortical actin cytoskeleton structure. For instance, cholesterol depletion induced stress fibre formation through Rho activation in both mesenchymal and epithelial cell lines (Qi *et al.*, 2009). However, other studies suggested less stable actin stress fibres after cholesterol depletion through the disorganization of phosphatidylinositol-4,5-bisphosphate (PIP_2) microdomains at the plasma membrane in both fibroblasts and lymphoblasts (Kwik *et al.*, 2003).

It is generally believed that annexins contribute to the architecture, functioning and structural organization of membranes through their binding to negatively charged phospholipids in a calcium-dependent manner, but also through protein-protein interactions with a variety of membrane-associated proteins. In addition, several annexins, including AnxA1, AnxA2 and AnxA6, have shown some affinity for cholesterol and cholesterol-enriched membranes (Ayala-Sanmartin, 2001; Hulce *et al.*, 2013). We and others showed that AnxA2 and AnxA6 translocate to detergent-resistant membranes (DRMs, membrane rafts) in a calcium-dependent manner (Gokhale *et al.*, 2005; Illien *et al.*, 2012), and were found enriched in caveolae (Schnitzer *et al.*, 1995; Calvo and Enrich, 2000). However, probably based on their strong affinity to negatively charged phospholipids, these annexins were also found in non-raft domains such as clathrin-coated pits, which are required for receptor-mediated endocytosis (Kamal *et al.*, 1998; Zobiack *et al.*, 2003).

In addition to its lipid-binding properties, we and others identified that AnxA6 acts as a scaffolding protein for signalling proteins such as PKCα and p120GAP (Grewal *et al.*, 2005; Rentero *et al.*, 2006; Koese *et al.*, 2013), but also interacts with cytoskeleton proteins such as actin and spectrin (Kamal *et al.*, 1998; Monastyrskaya *et al.*, 2009). This tethering ability of AnxA6 may indicate an anchoring role of AnxA6 to link lipid bilayers and cell cytoskeleton structure.

Although annexins have been proposed as membrane organizers since their discovery as calcium-dependent membrane-binding proteins more than three decades ago, experimental evidence for this hypothesis in living cells is still lacking. To address if AnxA6 alters membrane organization, we compared membrane order and protein clustering using the fluorescent dyes Laurdan and di-4-ANEPPDHQ, and super-resolution photoactivated localization microscopy (PALM), in live cells lacking or expressing AnxA6. Direct visualization of membrane lipid structure of living cells indicated that elevated AnxA6 expression significantly decreased membrane order through the regulation of cholesterol cellular homeostasis and actin cytoskeleton meshwork. These findings are in agreement with our previous data identifying reduced cholesterol levels at the plasma membrane upon AnxA6 up-regulation (Cubells *et al.*, 2007). Studies presented here provide the first evidence from live cells that a member of the annexins family, AnxA6, is capable of inducing changes in the membrane architecture.

Methods

Large unilamellar vesicle (LUV) preparation and fluorescence spectroscopy

LUVs mimicking the inner leaflet of the plasma membrane with and without cholesterol using a mix of PC, PS/PIP_2, PE and cholesterol (PC/PS or PIP_2/PE: 25/15/60 and PC/PS or PIP_2/PE/cholesterol: 17/12/52/19, weight ratio) were prepared by extrusion as previously described (Zibouche *et al.*, 2008) and Laurdan was added at a final concentration of 0.1%. Briefly, lipids were mixed together in chloroform. The solvent was removed under a stream of nitrogen and the residual solvent was removed under vacuum. Lipids were then resuspended in buffer A (40 mM HEPES pH 7, 30 mM KCl, 1 mM EGTA) at a final concentration of 1 mg·mL^{-1} by vortexing vigorously. The liposomes were then extruded by passing the suspension 21 times through a polycarbonate membrane with 0.1 μm pores (Avestin, Mannheim, Germany).

Fluorescence measurements were performed as described previously with a Cary fluorimeter (Varian, Agilent Technologies, Santa Clara, CA, USA) in cuvettes thermostated at 37°C (Maniti *et al.*, 2010). In five independent experiments, three spectra were recorded before and 7 min after addition of 5 μg purified AnxA6 to 5 μg LUVs in the presence of 500 μM Ca^{2+}. All fluorescence spectra were corrected for the baseline signal. Laurdan emission spectra were recorded from 400 to 600 nm using a 365 nm excitation wavelength, and its generalized polarization (GP) index was calculated according to the equation:

$$GP = (I_{(440)} - I_{(490)})/(I_{(440)} + I_{(490)})$$

where intensities at 440 and 490 nm ($I_{(440)}$ and $I_{(490)}$, respectively) represent the fluorescence intensities at the maximum emission wavelength in the ordered (440 nm) and disordered (490 nm) phases (Parasassi *et al.*, 1990). The means of three replicates from each independent experiment (n = 5) were used for the statistical analysis.

Cell culture, transfection and treatments

A431 adenocarcinoma cells were supplied by ATCC (CRL-1555; Middlesex, UK) and mouse embryonic fibroblast (MEF) cells were isolated from wild-type (WT) and AnxA6 knockout mice (Hawkins *et al.*, 1999) and immortalized by stable transfection of the SV40 large T antigen mammalian expression vector pBsSVD2005. Both cell types were grown in DMEM, 10% fetal calf serum, L-glutamine (2 mM), penicillin (100 U·mL^{-1}) and streptomycin (100 μg·mL^{-1}), and incubated at 37°C, 5% CO_2. The generation of stable AnxA6-expressing A431 cells has been described in detail (Grewal *et al.*, 2005). For transient transfection, A431 or MEF cells were transfected using Lipofectamine LTX (Life Technologies, Thermo Fisher Scientific, Inc., Waltham, CA, USA) following the manufacturer's instructions.

For di-4-ANEPPDHQ or PALM imaging, cells were treated with 1 μM (di-4-ANEPPDHQ) or 5 μM (PALM) LatB for 10 min, or with 10 mM mβCD for 30 min. For the addition of cholesterol, cells were incubated with 50 μg·mL^{-1} cholesterol for 2 h.

Fluorescence microscopy

For cholesterol imaging, cells were grown on glass coverslips, fixed with 4% paraformaldehyde (PFA) at 37°C, stained with 200 μg·mL^{-1} Filipin, mounted in Mowiol (Calbiochem, Merck Millipore, Darmstadt, Germany) and imaged with a Leica DMI 6000B epifluorescence inverted microscope (Leica Microsystems GmbH, Wetzlar, Germany) equipped with an HCX PLAN APO 63× oil immersion objective lens. For actin staining, cells were grown on glass coverslips, fixed and permeabilized with methanol for 2 min at –20°C, immunolabelled against β-actin and mounted in Mowiol (Calbiochem, Merck Millipore). Images were acquired with a Leica TCS-SL inverted spectral confocal microscope with a 63× oil immersion objective lens.

For di-4-ANEPPDHQ, live cells grown on glass coverslips were stained for 30 min at 37°C with 1.5 μM di-4-ANEPPDHQ in DMEM, and *in vivo* imaged as described previously (Owen *et al.*, 2012b) in a Leica TCS-SL inverted spectral confocal microscope with a 63× oil immersion objective lens. Di-4-ANEPPDHQ was excited at 488 nm and two simultaneous images were acquired at 540–580 and 620–700 nm channels. Di-4-ANEPPDHQ intensity images were converted into GP images (Gaus *et al.*, 2006; Owen *et al.*, 2012b), with each pixel calculated in ImageJ (Schneider *et al.*, 2012) from the two di-4-ANEPPDHQ intensity images according to the equation:

$$GP = (I_{(540-580)} - I_{(620-700)})/(I_{(540-580)} + I_{(620-700)})$$

GP distributions were obtained from the GP images histogram values and non-linearly fitted to one Gauss distributions using a custom-built macro in ImageJ (Owen *et al.*, 2012b). GP images were pseudocoloured. The induced membrane changes were estimated by the ΔGP ($GP_{treated} - GP_{untreated}$) value.

Cholesterol measurements

Total cellular cholesterol was determined using the Amplex™ Red Cholesterol Assay Kit (Molecular Probes, Thermo Fisher Scientific, Inc.) according to the manufacturer's instructions. Results were normalized to total cellular protein.

Photoactivated localization microscopy (PALM)

A431 and MEF cell lines were plated onto ozone-cleaned total internal reflection fluorescence (TIRF)-suitable 18 mm coverslips and transfected with Lck10-PS-CFP2 or Src15-PS-CFP2. Twenty-four hours after transfection, cells were treated with mβCD or LatB and fixed in 4% PFA at 37°C. Seven to ten PALM images were acquired on a TIRF microscope (ELYRA PS-1; Carl Zeiss MicroImaging, GmbH, Jena, Germany) with a 100× NA 1.46 oil immersion objective. Eight microwatts of 405 nm laser radiation was used for photo-conversion and 18 mW of 488 nm light was used for imaging of green-converted PS-CFP2. Fifteen thousand images were acquired per sample with a cooled, electron-multiplying charge-coupled device camera (iXon DU-897D; Andor Tech., Ltd., Belfast, UK) with an exposure time of 30 ms. Images were analysed with Zeiss ZEN 2010D software (Carl Zeiss MicroImaging GmbH). Drifting of the sample during acquisition was corrected relative to the position of surface-immobilized 100 nm colloidal gold beads (BB International, Cardiff, UK) placed on each sample.

PALM image analysis

Events from raw fluorescence intensity images were Gaussian and Laplace filtered, and were judged to be originated from single molecules when $I - M > 6S$, where I is event intensity, M is mean image intensity and S the SD of image intensity. The centre of each point-spread function was then calculated by fitting intensity profiles to a two-dimensional Gaussian distribution. After correction for sample drift with immobile colloidal gold bead markers, the x-y particle coordinates of each molecule were stored in a table. Two-dimensional molecular coordinates were cropped into non-overlapping regions of 3 μm × 3 μm in size. Stringent parameters for single molecule detection were applied as previously described, excluding molecules with localization precisions smaller than 30 nm and re-excited fluorophores from further analysis (Williamson *et al.*, 2011; Rossy *et al.*, 2013). Because individual fluorophores can undergo several 'blinking-cycles', we accounted for multiple blinks by selection of an appropriate off-gap, as published previously (Annibale *et al.*, 2011; Rossy *et al.*, 2013). Ripley's K function analysis and quantitative cluster maps were generated as described (Owen *et al.*, 2010). The Getis and Franklin's L function for local point pattern analysis was calculated with a cluster threshold of 60 ($L(r) > 60$) with the radial scale $r = 30$ nm, corresponding to approximately 30% of each region's cluster-map maximum (Owen *et al.*, 2013). Confidence intervals were generated by simulating 100 spatially random distributions with the same average molecular density as the data regions.

Isolation of DRMs

Isolation of DRMs was performed as described previously (Reverter *et al.*, 2011). Fractions were separated by SDS-PAGE and transferred to Immobilon-P membrane (Merck Millipore) followed by incubation with primary antibodies and the appropriate peroxidase-conjugated secondary antibodies and ECL detection (Amersham Biosciences, GE Healthcare Life Sciences, Pittsburgh, PA, USA).

Data analysis

Data were analysed for normality using the D'Agostiono-Pearson omnibus K^2 normality test (D'Agostino *et al.*, 1990) from Prism 5.02 software (GraphPad Software, Inc., La Jolla, CA, USA) to ensure Gaussian distribution and its suitability for further analysis. Statistical significance was determined by two-tailed unpaired Student's *t*-test or Bonferroni post-tested two-way ANOVA using Prism 5.02. Differences were considered statistically significant at $P < 0.05$. Graphs are given as bar plots ± SD or SEM as indicated in the figure legends.

Materials

DMEM was from Biological Industries (Kibbutz Beit-Haemek, Israel). Methyl-β-cyclodextrin (mβCD), egg yolk L-α-phos-

phatidylcholine (PC), egg yolk L-α-phosphatidylethanolamine (PE), brain L-α-glycerophosphatidyl-L-serine (PS) and cholesterol were purchased from Sigma-Aldrich (St. Louis, MO, USA). Latrunculin B (LatB) was purchased from Calbiochem (Merck Millipore). Brain L-α-phosphatidylinositol-4,5-bisphosphate (PIP_2) was from Avanti Polar Lipids (Alabaster, AL, USA). Laurdan, di-4-ANEPPDHPQ and Filipin were from Molecular Probes (Thermo Fisher Scientific, Inc.). Annexin A6 from pig brain was a kind gift of L.A. Pradel (Paris, France). Mouse monoclonal anti-β-actin and rabbit polyclonal antibody against GFP were from Abcam (Cambridge, UK). Rabbit polyclonal antibody against RFP was from Genscript (Piscataway, NJ, USA). HRP-conjugated secondary antibodies were from Bio-Rad Laboratories (Hercules, CA, USA). pBsSVD2005 (Addgene plasmid 21826) was a kind gift of D. Ron (Cambridge, UK).

For the generation of eGFP, monomeric Cherry (mCherry) and photoswitchable cyan fluorescent protein 2 (PS-CFP2) fusion proteins containing either the Lck10 or the Src15, sense and antisense oligonucleotides for the respective human sequences plus a spacer of four glycines were annealed and subcloned into the BamHI and EcoRI sites of pEGFP-N1 (Tanaka Bio Europe/Clontech, Saint-Germain-en-Laye, France), pmCherry-N1 (kindly provided by R.Y. Tsien, La Jolla, CA, USA) and pPS-CFP2-N1 (Evrogen, Moscow, Russia).

Results

AnxA6 changes membrane order in LUVs

The potential involvement of several annexin family members in the compartmentalization of membrane lipids and cortical actin cytoskeleton using *in vitro* vesicle and cellular models has been described previously (Illien *et al.*, 2012; Drucker *et al.*, 2013), supporting models of annexins as membrane organizers (Gerke *et al.*, 2005). This might involve the ability of annexins to bind negatively charged phospholipids as well as cholesterol. However, there is still a lack of an integrated model to explain how annexins may regulate the formation and/or maintenance of lipid microdomains.

Taking advantage of Laurdan, an environment-sensitive membrane probe, to label LUVs, we investigated whether the addition of AnxA6 could induce modification in membrane order in the presence or absence of cholesterol. Like other annexins, AnxA6 preferentially binds PS and other negatively charged phospholipids (Gerke *et al.*, 2005). AnxA6 may also show some affinity for PIP_2 *in vitro* (Enrich *et al.*, 2011; Hoque *et al.*, 2014), which is often enriched in specialized, cholesterol-rich domains (DRMs, lipid rafts) at the plasma membrane (Hayes *et al.*, 2004; Rescher and Gerke, 2004). Therefore, membrane order of PC and PE vesicles with PS or PIP_2 ± AnxA6 together with calcium and with or without cholesterol was compared.

As shown in Figure 1, the addition of cholesterol to PC/PS/PE and PC/PIP_2/PE LUVs strongly increased membrane order; Laurdan fluorescence intensity increased at 440 nm and decreased at 490 nm (compare the spectral shape of Figure 1B vs. 1A and Figure 1D vs. 1C), and the GP value [ratiometric function to quantify membrane order (Owen *et al.*, 2012b)] dramatically increased in those LUVs. In cholesterol-free Ld membranes (Figure 1A and C), AnxA6 induced a statistically significant increase in membrane order in both PS and PIP_2 LUVs (Figure 1A and C). At the same time, a statistically significant increase of membrane order (Lo) could be observed with the addition of purified AnxA6 to cholesterol-containing membranes (Figure 1B and D). Interestingly, addition of AnxA6 increased membrane order regardless whether LUVs contained PS or PIP_2. Taken together, these data indicate that AnxA6 is able to induce membrane lipid redistribution *in vitro*.

Annexin A6 regulates membrane order in living cells

To assess the possible role of AnxA6 in plasma membrane remodelling in living cells, we next examined the membrane order of two cellular models using: (i) the AnxA6-deficient epithelial adenocarcinoma cell line A431-WT and a well-characterized AnxA6-overexpressing A431 cell line (A431-A6) (Grewal *et al.*, 2005); and (ii) wild-type mesenchymal mouse embryonic fibroblasts (MEF-WT) and AnxA6 knockout MEFs (MEF-A6ko) derived from the AnxA6 knockout mice (Hawkins *et al.*, 1999).

Membrane order was assessed by labelling the plasma membrane of these cells with the fluorescent probe di-4-ANEPPDHQ (Figure 2A) (Owen *et al.*, 2012b). Di-4-ANEPPDHQ specifically labels the cell membranes (Figure 2A) and is associated with a spectral shift when membrane order decreases. The membrane order can be quantified by the ratiometric GP function (Figure 2B and C) (Owen *et al.*, 2012b), and the induced membrane changes can be estimated by the ΔGP ($GP_{treated} - GP_{untreated}$), where a positive ΔGP indicates an increase in membrane order and a negative ΔGP indicates a decrease in membrane order.

The comparison of ΔGP demonstrated that AnxA6 expression in A431 and MEF cells (A431-A6 and MEF-WT) induced a diminution in the plasma membrane order (Figure 2D and E). In line with published data, 30 min 10 mM mβCD treatment decreased membrane order in A431 and MEFs, independently of AnxA6 expression (Figure 2D and E). However, both up-regulation and loss of AnxA6 in A431-A6 and MEF-A6ko cells were associated with a significantly increased sensitivity towards mβCD compared with their respective controls. In contrast, the addition of exogenous cholesterol increased membrane order in both A431-WT and A431-A6 cells, restoring the membrane order perturbed by up-regulated AnxA6 expression (Supporting Information Fig. S1A). We have previously shown that elevated AnxA6 levels cause intracellular cholesterol imbalance, characterized by a strong reduction of the cholesterol levels at the plasma membrane (Cubells *et al.*, 2007). Filipin staining showed prominent cholesterol staining at the plasma membrane in AnxA6-deficient A431-WT (Cubells *et al.*, 2007) and MEF-A6ko cells (Supporting Information Fig. S1B), suggesting a redistribution of cholesterol to the plasma membrane in the absence of AnxA6. In line with previous data, plasma membrane cholesterol levels in cells with low/high AnxA6 levels did not correlate with total cholesterol levels in the two cell lines studied (Supporting Information Fig. S1C).

Next, we studied the contribution of the cortical actin cytoskeleton for plasma membrane organization in the pres-

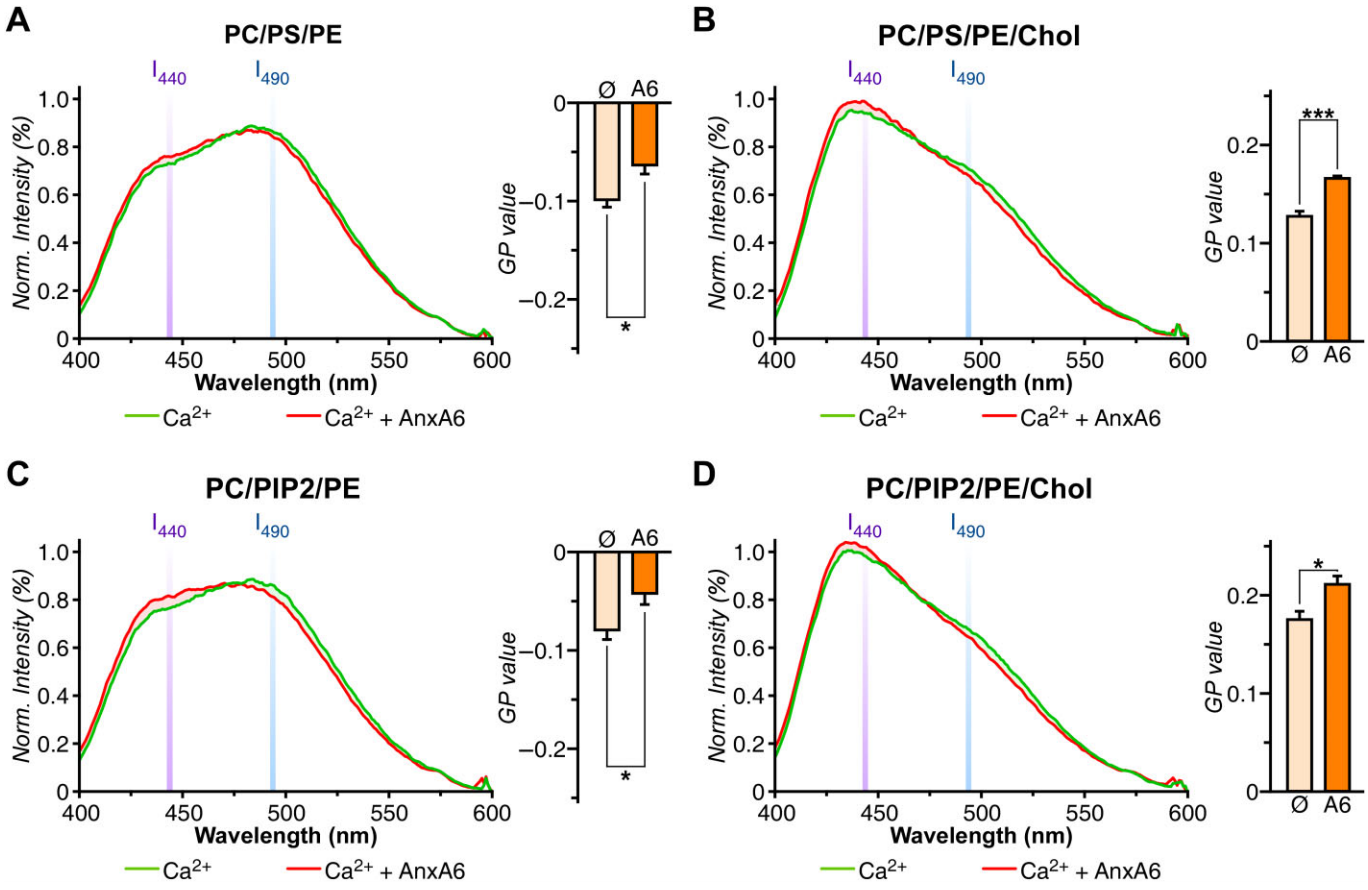

Figure 1

AnxA6 modifies membrane order in LUVs. Normalized fluorescence spectra of Laurdan stained (A) PC/PS/PE, (B) PC/PS/PE/Chol, (C) PC/PIP_2/PE and (D) PC/PIP_2/PE/Chol LUVs in the absence or presence of purified porcine AnxA6 (5 μg). Mean and SD graphical representation of its corresponding GP values. See Methods for the preparation of LUV details. The presented spectra are representative of five independent experiments (three replicates per condition for each experiment), where Lo (440 nm) and Ld (490 nm) emission wavelengths are represented. The means of three replicates from five independent experiments were used for statistical analysis. Unpaired Student's *t*-test showed statistically significant differences. *$P < 0.05$, **$P < 0.01$, ***$P < 0.001$. Chol, cholesterol.

ence or absence of AnxA6. Upon cortical actin network depolymerization after 10 min of 1 μM LatB treatment, we observed changes in membrane order of A431-A6 cells (Figure 2D). However, LatB induced a dramatic increment of membrane order in both MEF-WT and MEF-A6ko cell lines (Figure 2E). These findings correlated with AnxA6-dependent changes in actin cytoskeleton organization: (i) AnxA6 expression in A431 cells reduced cortical actin staining (arrowheads, Supporting Information Fig. S2). (ii) In contrast, AnxA6 expression in MEF cells increased stress fibres and reduced cell surface area.

Taken together, up-regulation of AnxA6 expression levels is associated with plasma membrane lipid redistributions, probably due to elevated AnxA6 levels causing intracellular cholesterol imbalance, in particular reducing cholesterol levels at the plasma membrane. This may contribute to create a microdomain environment that renders the plasma membrane in AnxA6-expressing cells more sensitive towards mβCD-induced lipid disorder. Furthermore, increased sensitivity towards actin-depolymerizing agents in our gain- and loss-of-function AnxA6 models may be indicative of AnxA6 providing a bridging function for the actin cytoskeleton to attach to the plasma membrane, with potentially drastic consequences for establishing membrane microdomain partitioning.

AnxA6-induced plasma membrane organization regulates clustering of raft and non-raft membrane proteins

Results presented above implied that AnxA6 contributed to membrane remodelling. To determine the effect of AnxA6-induced membrane order changes in protein domain partitioning at the plasma membrane in more detail, we next analysed the clustering of membrane-anchored fluorescent proteins expressed in the presence (A431-A6 and MEF-WT) or absence (A431-WT and MEF-A6ko) of AnxA6 by PALM super-resolution microscopy. Lck10 and Src15 membrane-targeting motifs were fused to the photoconvertible fluorescent protein PS-CFP2. Lck10 corresponds to the first 10 N-terminal amino acids of Lck, which contain a myristoylation and two palmitoylation groups and partitions into DRMs. In contrast, Src15 corresponds to the first 15 N-terminal residues of Src, which

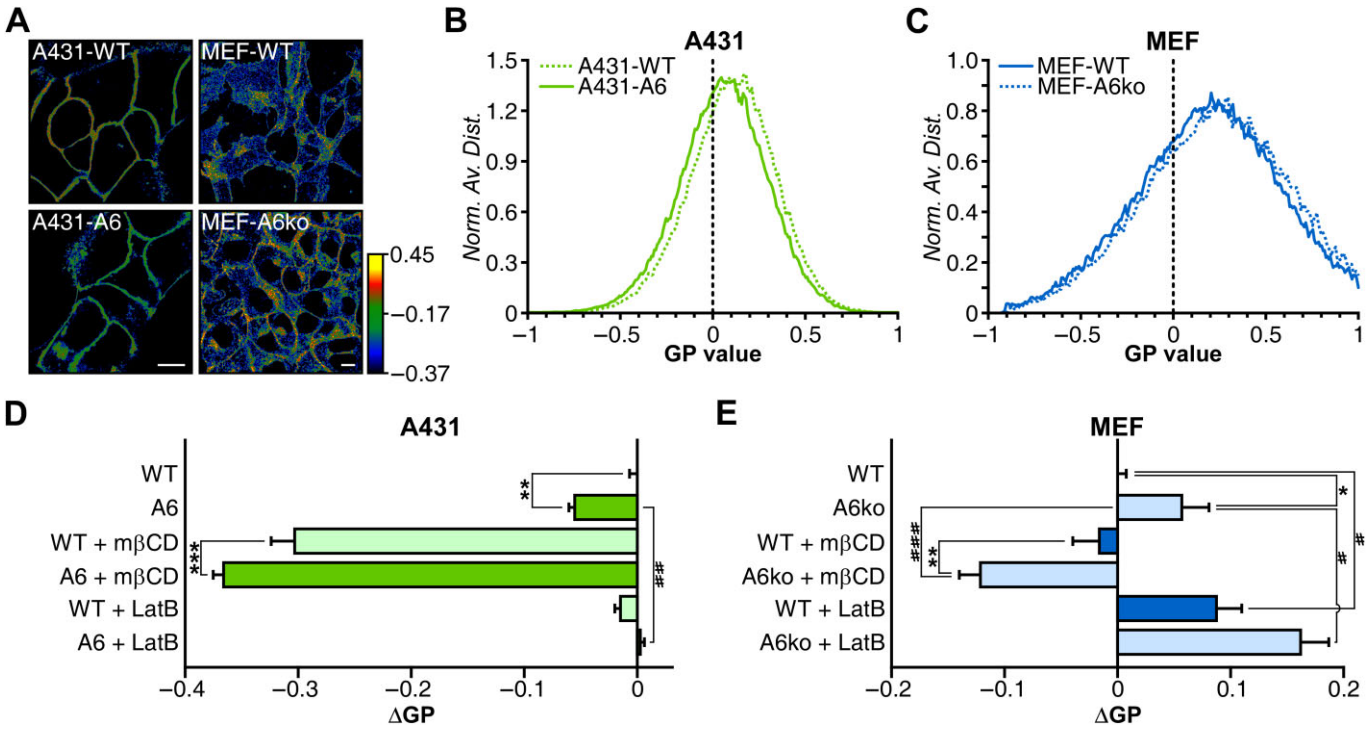

Figure 2

Membrane order of AnxA6-overexpressing A431 and AnxA6 knockout MEF cells. A431-WT, A431-A6, MEF-WT and MEF-A6ko cells were stained with 1.5 μg·mL^{-1} di-4-ANEPPDHQ for 30 min and imaged with a confocal microscope. (A) Representative GP pseudocoloured images of A431 and MEF cells. Bar, 10 μm. GP value histogram graphical representations of di-4-ANEPPDHQ stained (B) A431 and (C) MEF images from (A). (D) Mean and SD of A431-WT versus A431-A6 and (E) MEF-WT versus MEF-A6ko ΔGP representation under normal conditions, 30 min 10 mM mβCD and 10 min 5 μM LatB treatments of di-4-ANEPPDHQ stained images. The mean GP values of five images from five independent experiments were used to generate the ΔGP values for the statistical analysis. Two-way ANOVA tests were conducted on (C) and (D), and statistically significant interaction between AnxA6 levels and drug treatment ($F(2, 84) = 8.907$, $P = 0.0003$ in A431 cells; $F(2, 66) = 11.20$, $P < 0.0001$ in MEF cells) was determined. Bonferroni post-test analysis showed significant differences for drug treatment (#$P < 0.05$, ##$P < 0.01$, ###$P < 0.001$) and AnxA6 expression (*$P < 0.05$, **$P < 0.01$, ***$P < 0.001$).

contains a myristoylation group and several positively charged amino acids and is not enriched in DRMs but in Triton X-100 soluble fractions. In line with total cell lysate fractionation data, these motifs are targeted to raft (DRM) or to non-raft (TX-100 soluble) fractions of the plasma membrane respectively (Chichili and Rodgers, 2007) (Supporting Information Fig. S3).

The clustering level of Lck10 and Src15 membrane domain markers imaged by PALM microscopy was calculated using the Ripley's K function ($L(r)$-r), which indicates the degree of clustering (density of molecules) at a specific radius r (Owen *et al.*, 2010). Both these membrane domain markers clustered in A431 and MEF cells, with a clustering radius of r = 60 nm in all cases (Figures 3A,C and 4A,C). At this radius, we also analysed the percentage of molecules per cluster, the cluster density and the cluster radius (Figures 3B,D and 4B,D). A431 cells with and without AnxA6 displayed no significant changes in regard to raft marker clustering (Lck10, Figure 3A and B). However, Lck10 clustering, proportion of molecules in cluster and cluster density significantly increased in MEF-WT cells (Figure 4A and B). On the other hand, the expression of AnxA6 increased Src15 clustering, proportion of molecules in cluster and cluster density in both A431-A6 and MEF-WT cells, with slight increase in cluster radius (Figures 3C,D and 4C,D).

Hence, AnxA6 expression differentially affects the distribution of raft and non-raft markers depending on the cell type analysed. While AnxA6 increases membrane raft protein clustering only in MEF-WT, AnxA6 expression in both A431-A6 and MEF-WT increases non-lipid raft protein clustering.

AnxA6 modulates the regulatory role of cholesterol and cortical actin cytoskeleton in plasma membrane protein partitioning

Since the lipid raft model was proposed in 1997 by Ikonen and Simons (Simons and Ikonen, 1997), the cholesterol function on the protein partitioning at the plasma membrane has been studied extensively (Owen *et al.*, 2012a). As outlined above, we and others identified a role for AnxA6 in the regulation of cholesterol homeostasis (Enrich *et al.*, 2011), with elevated AnxA6 levels causing cholesterol accumulation in late endosomes, thereby reducing cholesterol at the Golgi complex and the plasma membrane (Cubells *et al.*, 2007). As

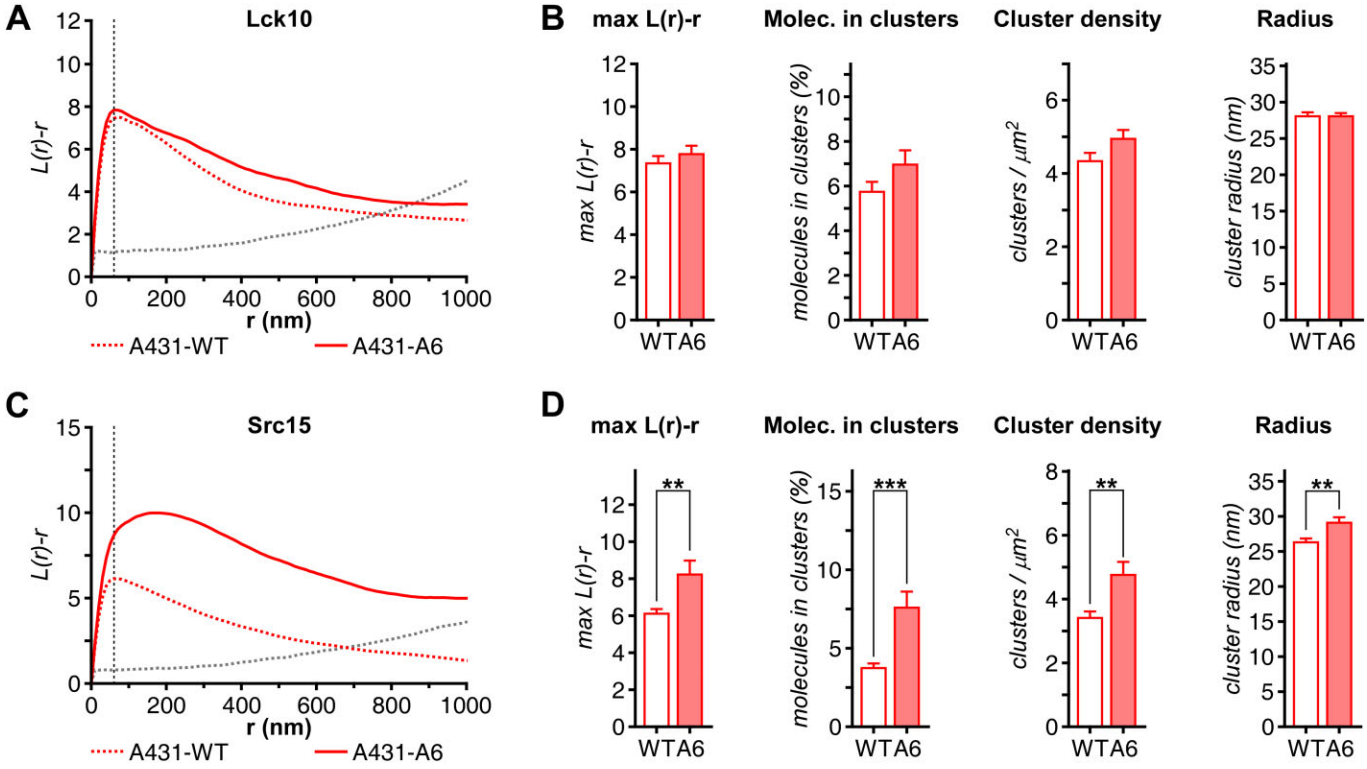

Figure 3

Cluster analysis of Lck10-PS-CFP2 and Src15-PS-CFP2 in A431-WT and A431-A6 cells. A431-WT and A431-A6 cells were transfected with (A and B) Lck10-PS-CFP2 and (C and D) Src15-PS-CFP2 and fixed 20 min with 4% PFA. PALM images were acquired and cluster analysis of 35–50 non-overlapping 3 × 3 µm regions at the plasma membrane from 7 to 10 PALM images was performed as explained in Materials and Methods. (A) Graphical representation of mean Ripley's K functions of 35–50 non-overlapping regions of Lck10-PS-CFP2 in A431-WT and A431-A6 cells. It reports the degree of clustering relative to a random distribution (indicated by the 95% CI, grey dotted line). (B) Graphical representation of mean ± SEM of maximum *L*(*r*)-*r* at radius = 60 nm, molecules in cluster, cluster density and cluster radius of Lck10-PS-CFP2 in A431-WT and A431-A6 cells. (C) Mean Ripley's K functions of 35–50 non-overlapping regions of Src15-PS-CFP2 in both A431-WT and A431-A6 cells. Grey dotted line, 95% CI. (D) Graphical representation of mean ± SEM of maximum *L*(*r*)-*r* at radius = 60 nm, molecules in cluster, cluster density and cluster radius of Src15-PS-CFP2 in A431-WT and A431-A6 cells. Unpaired Student's *t*-test showed statistically significant differences in (D). $^{**}P < 0.01$, $^{***}P < 0.001$.

shown above, AnxA6 modified membrane order of PS- and PIP_2-containing membrane bilayers in a calcium-dependent manner *in vitro* (Figure 1), but most strikingly, also in living cells (Figure 2). Furthermore, these AnxA6-induced changes in membrane order in live cells correlated with altered membrane-anchored raft and non-raft marker proteins partitioning at the plasma membrane (Figures 3 and 4).

To further assess the role of AnxA6 in cholesterol-dependent plasma membrane protein partitioning, Lck10- and Src15-PS-CFP2 transfected cells were treated with 30 min 10 mM mβCD, fixed and PALM images were acquired. The cluster analysis revealed that cholesterol depletion did not significantly affect Lck10 clustering in MEF-A6ko cells, but induced a broad Lck10 Ripley's K function curve, indicating higher heterogeneity of raft cluster size (Figure 5C, blue-dotted vs. red-dotted line; Supporting Information Fig. S4). In both AnxA6-expressing MEF-WT and A431-A6 cells, mβCD treatment significantly reduced Lck10 clustering and increased cluster size heterogeneity (Figure 5A and C, blue line; Supporting Information Fig. S4). On the other hand, mβCD treatment did not affect Src15 clustering of AnxA6-deficient A431-WT cells (Figure 5B, blue-dotted vs. red-dotted line; Supporting Information Fig. S4), but increased Src15 clustering, proportion of molecules in cluster, cluster density and cluster size in AnxA6-deficient MEF-A6ko cells (Figure 5D, blue-dotted line; Supporting Information Fig. S4). When we treated AnxA6-expressing A431-A6 cells with mβCD, Src15 clustering was comparable to non-treated A431-A6 cells (Figure 5B, blue vs. red line; Supporting Information Fig. S4). However, mβCD treatment of MEF-WT cells dropped Src15 clustering to levels observed in non-treated MEF-A6ko cells (Figure 5D, compare blue vs. red-dotted lines; Supporting Information Fig. S4).

Taken together, our PALM microscopy data further emphasize differential and cell-specific differences of AnxA6 on the cholesterol-sensitive microdomain distribution of raft and non-raft markers.

The function of the cortical actin meshwork in membrane protein partitioning and clustering has been examined extensively (Owen *et al.*, 2012a; Gomez-Llobregat *et al.*,

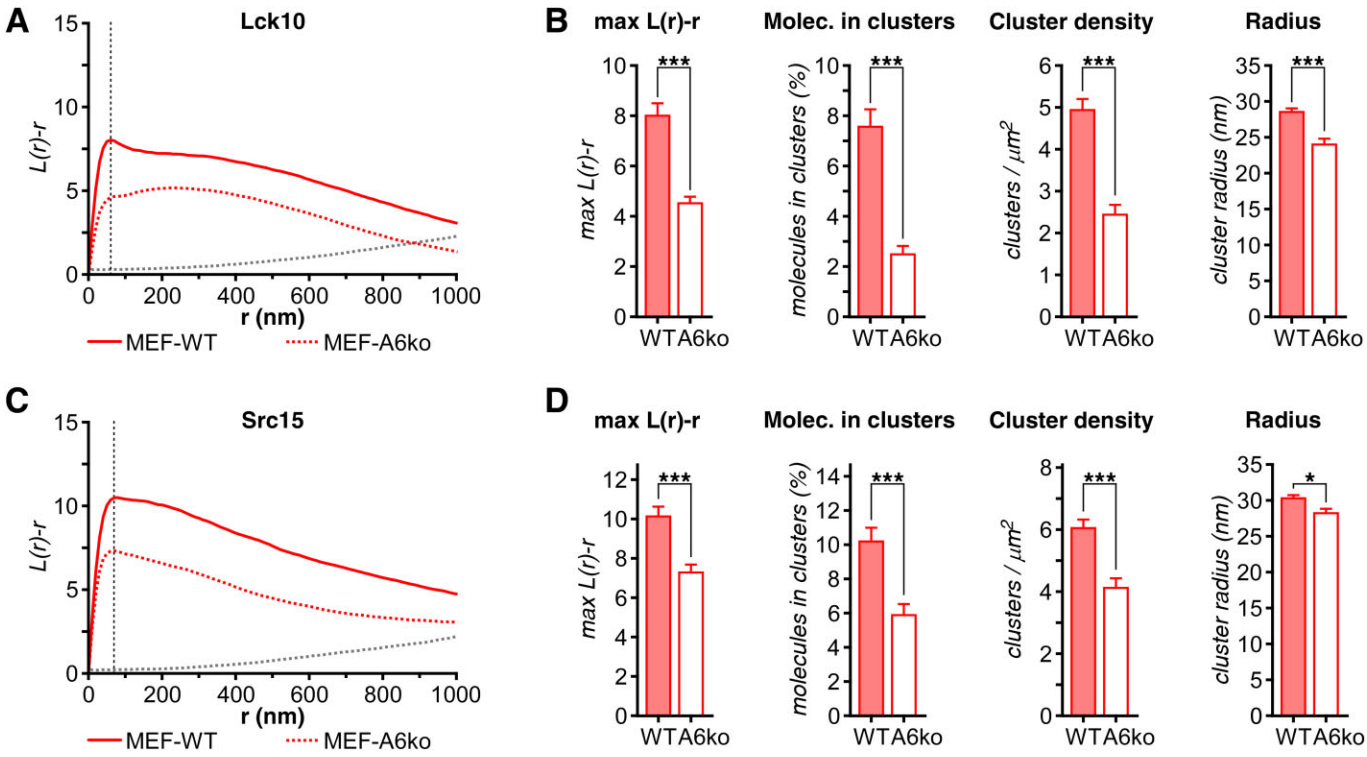

Figure 4

Cluster analysis of Lck10-PS-CFP2 and Src15-PS-CFP2 in MEF-WT and MEF-A6ko cells. MEF-WT and MEF-A6ko cells were transfected with (A and B) Lck10-PS-CFP2 and (C and D) Src15-PS-CFP2 and fixed 20 min with 4% PFA. PALM images were acquired and cluster analysis of 35–50 non-overlapping 3 × 3 µm regions at the plasma membrane from 7 to 10 PALM images was performed as explained in Materials and Methods. (A) Graphical representation of mean Ripley's K functions of 35–50 non-overlapping regions of Lck10-PS-CFP2 in both MEF-WT and MEF-A6ko cells. Grey dotted line, 95% CI. (B) Graphical representation of mean ± SEM of maximum *L*(*r*)-*r* at radius = 60 nm, molecules in cluster, cluster density and cluster radius of Lck10-PS-CFP2 in MEF-WT and MEF-A6ko cells. (C) Mean Ripley's K functions of 35–50 non-overlapping regions of Src15-PS-CFP2 in both MEF-WT and MEF-A6ko cells. Grey dotted line, 95% CI. (D) Graphical representation of mean ± SEM of maximum *L*(*r*)-*r* at radius = 60 nm, molecules in cluster, cluster density and cluster radius of Src15-PS-CFP2 in MEF-WT and MEF-A6ko cells. Unpaired Student's *t*-test showed statistically significant differences in (B) and (D). **P* < 0.05, ****P* < 0.001.

2013). To analyse if AnxA6 may contribute to cortical actin cytoskeleton-dependent compartmentalization of membrane-anchored proteins such as Lck10 and Src15, A431 and MEF ± AnxA6 cell lines transfected with fluorescent raft (Lck10) and non-raft (Src15) markers were treated with 5 µM LatB for 10 min, fixed and imaged by PALM microscopy. Cluster analysis of these PALM images revealed that actin cytoskeleton disruption did not significantly affect Lck10 clustering in AnxA6-deficient A431-WT cells, but increased cluster heterogeneity in MEF-A6ko fibroblasts (Figure 5A and C, green-dotted vs. red-dotted line; Supporting Information Fig. S4). In contrast, AnxA6 expression in A431-A6 and MEF-WT correlated with LatB treatment inducing Lck10 clustering (proportion of molecules in cluster, cluster density and cluster size) (Figure 5A and C, green line; Supporting Information Fig. S4). On the other hand, LatB treatment induced Src15 clustering in both A431-WT and MEF-A6ko cells (Figure 5B and D, green-dotted vs. red-dotted line; Supporting Information Fig. S4). The expression of AnxA6 in LatB-treated A431 cells reduced Src15 clustering to almost the clustering levels of untreated A431-WT cells (Figure 5B, green vs. red-dotted line; Supporting Information Fig. S4). In MEF-WT, the presence of AnxA6 was associated with slightly more Src15 clustering, proportion of molecules in cluster, cluster density and cluster size than in LatB-treated MEF-A6ko fibroblasts (Figure 5D, green vs. red line; Supporting Information Fig. S4).

Altogether, these results highlight that differential expression levels of AnxA6 not only alter the cholesterol-sensitive distribution of raft and non-raft proteins, but can also modulate the actin-dependent microdomain environment in a cell-specific manner.

Discussion and conclusions

Utilizing two gain- and loss-of-function cellular models for AnxA6, this study provides the first evidence from live cells that members of the annexin family have the ability to remodel plasma membrane order. Results presented here strongly suggest that AnxA6 modulates plasma membrane order through two different mechanisms: (i) directly affecting phospholipid bilayer organization and the actin cortical cytoskeleton; and (ii) indirectly through alterations in cholesterol homeostasis, thereby inducing plasma membrane cholesterol depletion and plasma membrane order diminution.

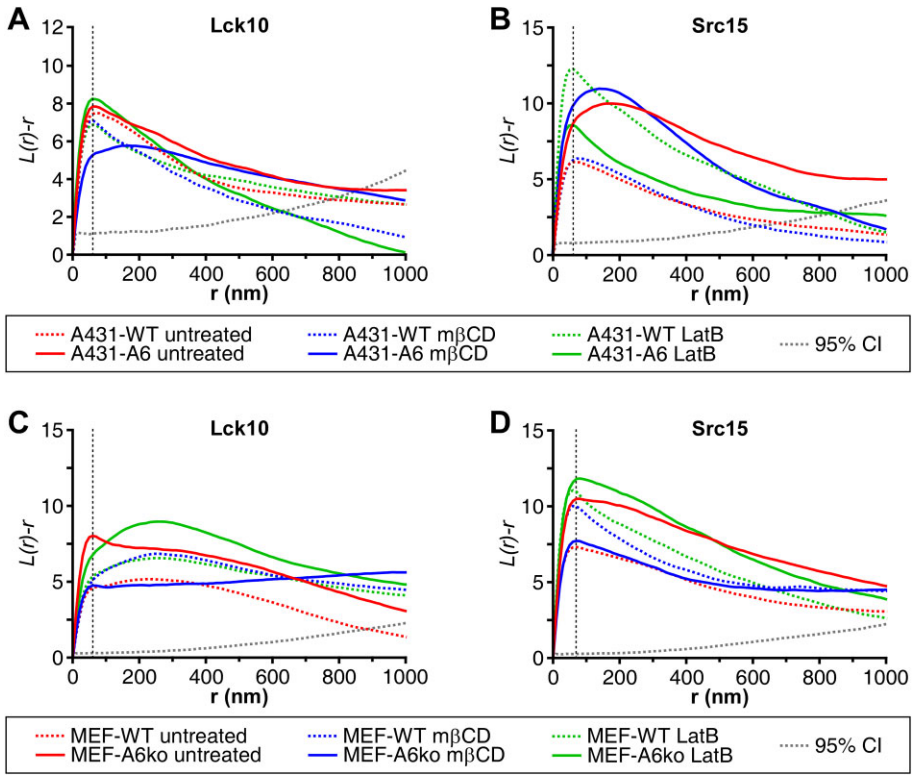

Figure 5

Ripley's K function of Lck10-PS-CFP2 and Src15-PS-CFP2 in mβCD and LatB-treated A431 and MEF cells. Mean Ripley's K function graphical representations of 35–50 non-overlapping 3 × 3 μm regions at the plasma membrane from 7 to 10 PALM images of (A and B) A431-WT and A431-A6 and (C and D) MEF-WT and MEF-A6ko of (A and C) Lck10-PS-CFP2 and (B and D) Src15-PS-CFP2 transfected cells. Graphs show the mean of Ripley's K functions under normal conditions, 10 mM mβCD and 5 μM LatB treatments. Grey dotted line, 95% CIs.

AnxA6 is well known to play a role in calcium homeostasis, membrane traffic and membrane organization. Negatively charged phospholipids [phosphatidylserine (PS), phosphatidylinositol, phosphatidic acid] are the preferred binding partners of annexins. It has been suggested that, despite calcium-dependent interaction with anionic phospholipids, AnxA6 displays calcium-independent cholesterol-binding properties (de Diego *et al.*, 2002). In addition, AnxA6 also shows affinity for PE and arachidonic acid (Edwards and Crumpton, 1991), which are enriched in membrane rafts and generated by cytoplasmic phospholipase A_2 ($cPLA_2$) (Brown *et al.*, 2003). Apart from the role in phospholipid reorganization and membrane aggregation, AnxA6 expression also regulates intracellular cholesterol homeostasis (Grewal *et al.*, 2010). Cells with elevated AnxA6 levels are characterized by an accumulation of cholesterol in late endosomes, with a consequent cholesterol diminution at the plasma membrane and Golgi apparatus, which inhibits caveolin-1 transport to the plasma membrane (Cubells *et al.*, 2007). Interestingly, cholesterol depletion in the Golgi of AnxA6-expressing cells interferes with the recruitment and activity of $cPLA_2$ at the trans-Golgi-network (TGN) (Cubells *et al.*, 2008). Given that $cPLA_2$ is required to drive cholesterol-dependent formation and transport of secretory vesicles from the TGN to the plasma membrane, this might further contribute to changes in membrane order at the cell surface.

A role for cholesterol to stimulate the binding of AnxA6 to liposomes *in vitro* (Ayala-Sanmartin, 2001) and changes in cholesterol and/or pH stimulating Ca^{2+}-independent interactions of AnxA6 with endosomal and cell surface membranes had already been observed in earlier studies (de Diego *et al.*, 2002; Monastyrskaya *et al.*, 2009). AnxA6 has been postulated as a *bona fide* cholesterol-binding protein; *in vitro* binding studies identified tryptophan-343 (W343) within the linker region of AnxA6 as important for the proposed interaction between recombinant AnxA6 and cholesterol (Domon *et al.*, 2010). More recently, a comprehensive proteome-wide mapping of cholesterol-interacting proteins in mammalian cells recognized AnxA6 as a potential cholesterol-binding protein (Hulce *et al.*, 2013). Interestingly, while AnxA6 has been linked to cholesterol homeostasis, similar modes of action have not been made for other annexins like AnxA2, indicating different mechanisms of AnxA2 and AnxA6 to affect plasma membrane order (Illien *et al.*, 2012).

In Figure 6, we propose a model that summarizes and links AnxA6 expression with cholesterol- and actin-mediated structural and functional changes at the plasma membrane. This model outlines two different plasma membrane domain distributions depending on cellular cholesterol levels and cortical actin cytoskeleton meshwork features. In MEF cells, the cortical actin cytoskeleton forms corrals where the Lo raft domains are confined. This hypothesis is in agreement with

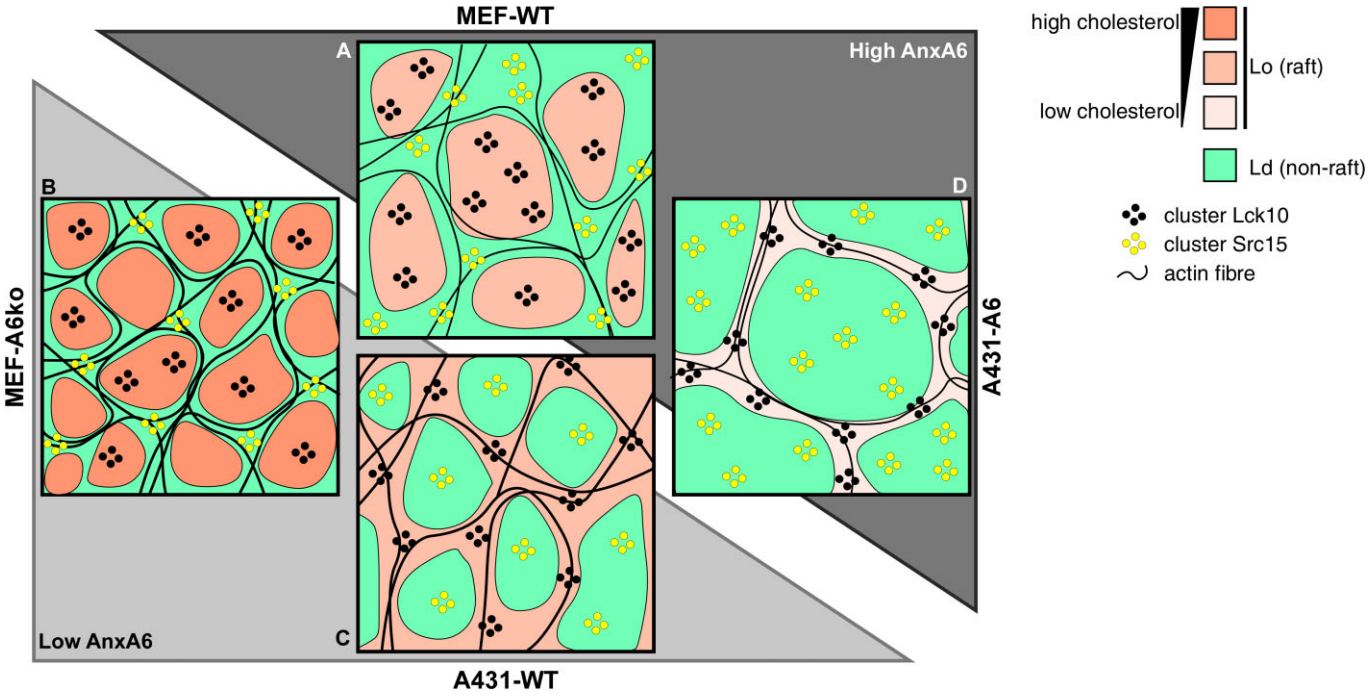

Figure 6

Proposed model for AnxA6-induced membrane organization. The proposed model suggests that fibroblasts plasma membrane (A) has lipid raft confined into actin fibre corrals due to its cholesterol content and its cortical actin cytoskeleton. (B) When AnxA6 is knocked out, higher plasma membrane cholesterol content and a prominent cortical actin cytoskeleton can be observed, which could drive domain partitioning of both Lo and Ld phases. On the other hand, epithelial cells (C and D) might have non-rafts confined into corrals where cortical actin cytoskeleton determines corral size and cluster partitioning. (D) In this setting, AnxA6 expression may induce diminution of cortical actin cytoskeleton and plasma membrane cholesterol, allowing larger non-raft Ld domains.

recent findings that describe, using fluorescent correlation spectrometry and stimulated emission depletion super-resolution microscopy, membrane partitioning into Lo-enriched domains surrounded by Ld-enriched domains that correlate with actin fibres (Honigmann *et al.*, 2014). In both models, the degree of the actin meshwork density will determine the corral size, and the level of membrane cholesterol and other raftophilic lipid moieties will determine the different membrane phase proportions. In A431 cells, however, cortical actin cytoskeleton delimits Ld non-raft domains into corrals, with the Lo membrane phase associated with the actin filaments. Experimental data supporting this hypothesis, using a phasor approach to fluorescence lifetime imaging microscopy data analysis and 7-ketocholesterol treatment, allowed us to propose a model where, in reduced plasma membrane order conditions, Ld phase is present in the corral lumen while the Lo raft phase is associated with actin filaments (Owen *et al.*, 2012c). The proposed model here suggests that the regulation of cholesterol levels, other raftophilic lipid moieties and/or the actin cytoskeleton meshwork, by means of AnxA6 and other membrane regulators or even specific drugs such as mβCD or LatB, might modulate the plasma membrane structure and partitioning. In addition, fluctuations in intracellular calcium levels are well known to strongly affect the membrane-binding ability of AnxA6 *in vitro*, but also in cellular models. For instance, we showed that calcium ionophores, but also activation of epidermal growth factor receptor (EGFR), which triggers local intracellular calcium concentration increase, induces AnxA6 translocation to the plasma membrane (Vila de Muga *et al.*, 2009; Grewal *et al.*, 2010). Hence, a combination of cholesterol, actin and calcium-driven events probably enables AnxA6 to not only affect the membrane order locally, but also to affect recruitment of signalling proteins to the plasma membrane. In line with this hypothesis, AnxA6 promotes calcium-dependent membrane recruitment of the GTPase activating protein p120GAP (Grewal *et al.*, 2005) as well as PKCα (Koese *et al.*, 2013). This is associated with AnxA6 interacting with active H-Ras and EGFR, promoting EGF-inducible Ras and EGFR inactivation in a calcium-dependent manner (Vila de Muga *et al.*, 2009; Koese *et al.*, 2013). One can envisage that the dual role of AnxA6 affecting membrane order through cholesterol- and actin-dependent events identified here, together with calcium-sensitive AnxA6 membrane association, modulates the recruitment of signalling proteins, and consequently strength and duration of cellular signalling.

We and others have shown different AnxA6 functions regulating important cellular/physiological events such as endocytosis, exocytosis and cell migration, where membrane partitioning is considered essential. Firstly, AnxA6 is located at clathrin-coated pits and caveolae at the plasma membrane (Calvo and Enrich, 2000), specific membrane structures characterized by Ld and Lo phases respectively. Anderson and

co-workers, based on AnxA6 interacting with spectrin, proposed a role for AnxA6 in receptor-mediated endocytosis (Kamal *et al.*, 1998). Upon AnxA6 binding to spectrin, calpain I cleaves spectrin and 'opens' the actin cytoskeleton facilitating the endocytosis. These AnxA6-dependent dynamic changes in membrane–cytoskeleton interaction are likely to involve changes in membrane order.

Secondly, currently available data suggest that AnxA6 probably inhibits the secretory pathway (Creutz, 1992; Donnelly and Moss, 1997; Podszywalow-Bartnicka *et al.*, 2010). Our recent findings are in line with this concept as we identified a significant diminution of retrograde transport of vesicular stomatitis virus G protein transport from the cell surface to the TGN in cells with up-regulated AnxA6 levels (Cubells *et al.*, 2007). Furthermore, high levels of AnxA6 interfered with cholesterol-sensitive and t-SNARE (SNAP23 and syntaxin-4) dependent secretion of cargo (fibronectin, TNF-α) (Reverter *et al.*, 2011).

Finally, our most recent data provide novel molecular insights into our understanding of constitutive protein trafficking at the TGN/endosomal boundaries and identify the delivery of late endosomal cholesterol to the Golgi as a new pathway linking cholesterol with t-SNARE functioning and integrin recycling (Reverter *et al.*, 2014).

Future studies will have to determine whether AnxA6 expression levels and its influence in the remodelling of membrane microdomains are a common determinant for cholesterol regulation of t-SNARE localization, assembly and functioning in various cellular processes and cell types.

Acknowledgements

This study was supported by grants BFU2012-36272 and CSD2009-00016 from Ministerio de Economía y Competitividad (MINECO, Spain) and PI042182 from Fundació Marató TV3 (Spain) to C. E. K. G. would like to acknowledge funding from the National Health and Medical Research Council of Australia (NHMRC; 1059278, 1022182 and 1037320) and the Australian Research Council (ARC; CE140100011). T. G. is supported by the NHMRC of Australia (510294) and the University of Sydney (2010-02681). F. T. is supported by MINECO (BFU2012-38259). We are thankful to M. Calvo (Centres Científics i Tecnològics, Universitat de Barcelona) for her help in confocal microscopy, and M. Molinos for technical assistance. A. A. G. and M. R. are grateful to MEC for a short-term fellowship at the Center for Vascular Research, University of New South Wales in Sydney, Australia.

Author contributions

A. A-G.: PALM experiments and biochemistry. S. V. d. M.: Di-4-ANEPPDHQ experiments. D. M. O. and D. W.: PALM quantification. A. M.: Lck10 and Src15 cloning. A. G-M.: Immunocytochemistry. M. R.: Cholesterol quantification. M. H. and R. C.: Biochemistry experiments. R. C.: Lck10 and Src15 cloning. F. T.: Discussion of results. T. G.: Discussion and proofreading. K. G.: PALM experiments design. J. A-S.: LUV experiments and discussion. C. E.: Financial support, discussion and proofreading. C. R.: Experiment design, discussion of results and writing the paper.

Conflict of interest

The authors disclose no conflicts.

References

Alexander SPH, Benson HE, Faccenda E, Pawson AJ, Sharman JL, Spedding M *et al* (2013a). The Concise Guide to PHARMACOLOGY 2013/14: Enzymes. Br J Pharmacol 170: 1797–1867.

Alexander SPH, Benson HE, Faccenda E, Pawson AJ, Sharman JL, Spedding M *et al* (2013b). The Concise Guide to PHARMACOLOGY 2013/14: Catalytic Receptors. Br J Pharmacol 170: 1676–1705.

Annibale P, Vanni S, Scarselli M, Rothlisberger U, Radenovic A (2011). Quantitative photo activated localization microscopy: unraveling the effects of photoblinking. PLoS ONE 6: e22678.

Ayala-Sanmartin J (2001). Cholesterol enhances phospholipid binding and aggregation of annexins by their core domain. Biochem Biophys Res Commun 283: 72–79.

Brown WJ, Chambers K, Doody A (2003). Phospholipase A2 (PLA2) enzymes in membrane trafficking: mediators of membrane shape and function. Traffic 4: 214–221.

Calvo M, Enrich C (2000). Biochemical analysis of a caveolae-enriched plasma membrane fraction from rat liver. Electrophoresis 21: 3386–3395.

Chichili GR, Rodgers W (2007). Clustering of membrane raft proteins by the actin cytoskeleton. J Biol Chem 282: 36682–36691.

Creutz CE (1992). The annexins and exocytosis. Science 258: 924–931.

Cubells L, Vila de Muga S, Tebar F, Wood P, Evans R, Ingelmo-Torres M *et al.* (2007). Annexin A6-induced alterations in cholesterol transport and caveolin export from the Golgi complex. Traffic 8: 1568–1589.

Cubells L, Vila de Muga S, Tebar F, Bonventre JV, Balsinde J, Pol A *et al.* (2008). Annexin A6-induced inhibition of cytoplasmic phospholipase A2 is linked to caveolin-1 export from the Golgi. J Biol Chem 283: 10174–10183.

D'Agostino RB, Belanger A, D'Agostino RBJ (1990). A suggestion for using powerful and informative tests of normality. Am Stat 44: 316–321.

de Diego I, Schwartz F, Siegfried H, Dauterstedt P, Heeren J, Beisiegel U *et al.* (2002). Cholesterol modulates the membrane binding and intracellular distribution of annexin 6. J Biol Chem 277: 32187–32194.

Domon MM, Matar G, Strzelecka-Kiliszek A, Bandorowicz-Pikula J, Pikula S, Besson F (2010). Interaction of annexin A6 with cholesterol rich membranes is pH-dependent and mediated by the sterol OH. J Colloid Interface Sci 346: 436–441.

Donnelly SR, Moss SE (1997). Annexins in the secretory pathway. Cell Mol Life Sci 53: 533–538.

Drucker P, Pejic M, Galla HJ, Gerke V (2013). Lipid segregation and membrane budding induced by the peripheral membrane binding protein annexin A2. J Biol Chem 288: 24764–24776.

Edwards HC, Crumpton MJ (1991). Ca(2+)-dependent phospholipid and arachidonic acid binding by the placental annexins VI and IV. Eur J Biochem 198: 121–129.

Enrich C, Rentero C, de Muga SV, Reverter M, Mulay V, Wood P *et al*. (2011). Annexin A6-Linking Ca(2+) signaling with cholesterol transport. Biochim Biophys Acta 1813: 935–947.

Gaus K, Zech T, Harder T (2006). Visualizing membrane microdomains by Laurdan 2-photon microscopy. Mol Membr Biol 23: 41–48.

Gerke V, Creutz CE, Moss SE (2005). Annexins: linking Ca2+ signalling to membrane dynamics. Nat Rev Mol Cell Biol 6: 449–461.

Gokhale NA, Abraham A, Digman MA, Gratton E, Cho W (2005). Phosphoinositide specificity of and mechanism of lipid domain formation by annexin A2-p11 heterotetramer. J Biol Chem 280: 42831–42840.

Gomez-Llobregat J, Buceta J, Reigada R (2013). Interplay of cytoskeletal activity and lipid phase stability in dynamic protein recruitment and clustering. Sci Rep 3: 2608.

Grewal T, Evans R, Rentero C, Tebar F, Cubells L, de Diego I *et al*. (2005). Annexin A6 stimulates the membrane recruitment of p120GAP to modulate Ras and Raf-1 activity. Oncogene 24: 5809–5820.

Grewal T, Koese M, Rentero C, Enrich C (2010). Annexin A6-regulator of the EGFR/Ras signalling pathway and cholesterol homeostasis. Int J Biochem Cell Biol 42: 580–584.

Hawkins TE, Roes J, Rees D, Monkhouse J, Moss SE (1999). Immunological development and cardiovascular function are normal in annexin VI null mutant mice. Mol Cell Biol 19: 8028–8032.

Hayes MJ, Rescher U, Gerke V, Moss SE (2004). Annexin-actin interactions. Traffic 5: 571–576.

Head BP, Patel HH, Insel PA (2014). Interaction of membrane/lipid rafts with the cytoskeleton: impact on signaling and function: membrane/lipid rafts, mediators of cytoskeletal arrangement and cell signaling. Biochim Biophys Acta 1838: 532–545.

Honigmann A, Sadeghi S, Keller J, Hell SW, Eggeling C, Vink R (2014). A lipid bound actin meshwork organizes liquid phase separation in model membranes. eLife 3: e01671.

Hoque M, Rentero C, Cairns R, Tebar F, Enrich C, Grewal T (2014). Annexins – scaffolds modulating PKC localization and signaling. Cell Signal 26: 1213–1225.

Hulce JJ, Cognetta AB, Niphakis MJ, Tully SE, Cravatt BF (2013). Proteome-wide mapping of cholesterol-interacting proteins in mammalian cells. Nat Methods 10: 259–264.

Illien F, Piao HR, Coue M, di Marco C, Ayala-Sanmartin J (2012). Lipid organization regulates annexin A2 Ca(2+)-sensitivity for membrane bridging and its modulator effects on membrane fluidity. Biochim Biophys Acta 1818: 2892–2900.

Jacobson K, Mouritsen OG, Anderson RG (2007). Lipid rafts: at a crossroad between cell biology and physics. Nat Cell Biol 9: 7–14.

Kamal A, Ying Y, Anderson RG (1998). Annexin VI-mediated loss of spectrin during coated pit budding is coupled to delivery of LDL to lysosomes. J Cell Biol 142: 937–947.

Koese M, Rentero C, Kota BP, Hoque M, Cairns R, Wood P *et al*. (2013). Annexin A6 is a scaffold for PKCalpha to promote EGFR inactivation. Oncogene 32: 2858–2872.

Kusumi A, Koyama-Honda I, Suzuki K (2004). Molecular dynamics and interactions for creation of stimulation-induced stabilized rafts from small unstable steady-state rafts. Traffic 5: 213–230.

Kwik J, Boyle S, Fooksman D, Margolis L, Sheetz MP, Edidin M (2003). Membrane cholesterol, lateral mobility, and the phosphatidylinositol 4,5-bisphosphate-dependent organization of cell actin. Proc Natl Acad Sci U S A 100: 13964–13969.

Lillemeier BF, Pfeiffer JR, Surviladze Z, Wilson BS, Davis MM (2006). Plasma membrane-associated proteins are clustered into islands attached to the cytoskeleton. Proc Natl Acad Sci U S A 103: 18992–18997.

Maniti O, Alves I, Trugnan G, Ayala-Sanmartin J (2010). Distinct behaviour of the homeodomain derived cell penetrating peptide penetratin in interaction with different phospholipids. PLoS ONE 5: e15819.

Monastyrskaya K, Babiychuk EB, Hostettler A, Wood P, Grewal T, Draeger A (2009). Plasma membrane-associated annexin A6 reduces Ca2+ entry by stabilizing the cortical actin cytoskeleton. J Biol Chem 284: 17227–17242.

Nicolson GL (2014). The Fluid-Mosaic Model of Membrane Structure: still relevant to understanding the structure, function and dynamics of biological membranes after more than 40 years. Biochim Biophys Acta 1838: 1451–1466.

Owen DM, Rentero C, Rossy J, Magenau A, Williamson D, Rodriguez M *et al*. (2010). PALM imaging and cluster analysis of protein heterogeneity at the cell surface. J Biophotonics 3: 446–454.

Owen DM, Magenau A, Williamson D, Gaus K (2012a). The lipid raft hypothesis revisited–new insights on raft composition and function from super-resolution fluorescence microscopy. Bioessays 34: 739–747.

Owen DM, Rentero C, Magenau A, Abu-Siniyeh A, Gaus K (2012b). Quantitative imaging of membrane lipid order in cells and organisms. Nat Protoc 7: 24–35.

Owen DM, Williamson DJ, Magenau A, Gaus K (2012c). Sub-resolution lipid domains exist in the plasma membrane and regulate protein diffusion and distribution. Nat Commun 3: 1256.

Owen DM, Magenau A, Williamson DJ, Gaus K (2013). Super-resolution imaging by localization microscopy. Methods Mol Biol 950: 81–93.

Parasassi T, De Stasio G, d'Ubaldo A, Gratton E (1990). Phase fluctuation in phospholipid membranes revealed by Laurdan fluorescence. Biophys J 57: 1179–1186.

Parton RG, Richards AA (2003). Lipid rafts and caveolae as portals for endocytosis: new insights and common mechanisms. Traffic 4: 724–738.

Pawson AJ, Sharman JL, Benson HE, Faccenda E, Alexander SP, Buneman OP *et al*.; NC-IUPHAR (2014). The IUPHAR/BPS Guide to PHARMACOLOGY: an expert-driven knowledge base of drug targets and their ligands. Nucleic Acids Res 42 (Database Issue): D1098–1106.

Podszywalow-Bartnicka P, Kosiorek M, Piwocka K, Sikora E, Zablocki K, Pikula S (2010). Role of annexin A6 isoforms in catecholamine secretion by PC12 cells: distinct influence on calcium response. J Cell Biochem 111: 168–178.

Qi M, Liu Y, Freeman MR, Solomon KR (2009). Cholesterol-regulated stress fiber formation. J Cell Biochem 106: 1031–1040.

Rentero C, Evans R, Wood P, Tebar F, Vila de Muga S, Cubells L *et al*. (2006). Inhibition of H-Ras and MAPK is compensated by PKC-dependent pathways in annexin A6 expressing cells. Cell Signal 18: 1006–1016.

Rescher U, Gerke V (2004). Annexins – unique membrane binding proteins with diverse functions. J Cell Sci 117 (Pt 13): 2631–2639.

Reverter M, Rentero C, de Muga SV, Alvarez-Guaita A, Mulay V, Cairns R *et al*. (2011). Cholesterol transport from late endosomes to the Golgi regulates t-SNARE trafficking, assembly, and function. Mol Biol Cell 22: 4108–4123.

Reverter M, Rentero C, Garcia-Melero A, Hoque M, Vila de Muga S, Alvarez-Guaita A *et al*. (2014). Cholesterol regulates Syntaxin 6 trafficking at trans-Golgi network endosomal boundaries. Cell Rep 7: 883–897.

Ritchie K, Iino R, Fujiwara T, Murase K, Kusumi A (2003). The fence and picket structure of the plasma membrane of live cells as revealed by single molecule techniques (Review). Mol Membr Biol 20: 13–18.

Rossy J, Owen DM, Williamson DJ, Yang Z, Gaus K (2013). Conformational states of the kinase Lck regulate clustering in early T cell signaling. Nat Immunol 14: 82–89.

Schneider CA, Rasband WS, Eliceiri KW (2012). NIH Image to ImageJ: 25 years of image analysis. Nat Methods 9: 671–675.

Schnitzer JE, Liu J, Oh P (1995). Endothelial caveolae have the molecular transport machinery for vesicle budding, docking, and fusion including VAMP, NSF, SNAP, annexins, and GTPases. J Biol Chem 270: 14399–14404.

Simons K, Ikonen E (1997). Functional rafts in cell membranes. Nature 387: 569–572.

Simons K, Toomre D (2000). Lipid rafts and signal transduction. Nat Rev Mol Cell Biol 1: 31–39.

Singer SJ, Nicolson GL (1972). The fluid mosaic model of the structure of cell membranes. Science 175: 720–731.

Sugano K, Kansy M, Artursson P, Avdeef A, Bendels S, Di L *et al*. (2010). Coexistence of passive and carrier-mediated processes in drug transport. Nat Rev Drug Discov 9: 597–614.

Vila de Muga S, Timpson P, Cubells L, Evans R, Hayes TE, Rentero C *et al*. (2009). Annexin A6 inhibits Ras signalling in breast cancer cells. Oncogene 28: 363–377.

Williamson DJ, Owen DM, Rossy J, Magenau A, Wehrmann M, Gooding JJ *et al*. (2011). Pre-existing clusters of the adaptor Lat do not participate in early T cell signaling events. Nat Immunol 12: 655–662.

Zibouche M, Vincent M, Illien F, Gallay J, Ayala-Sanmartin J (2008). The N-terminal domain of annexin 2 serves as a secondary binding site during membrane bridging. J Biol Chem 283: 22121–22127.

Zobiack N, Rescher U, Ludwig C, Zeuschner D, Gerke V (2003). The annexin 2/S100A10 complex controls the distribution of transferrin receptor-containing recycling endosomes. Mol Biol Cell 14: 4896–4908.

Zocher F, van der Spoel D, Pohl P, Hub JS (2013). Local partition coefficients govern solute permeability of cholesterol-containing membranes. Biophys J 105: 2760–2770.

Supporting information

Additional Supporting Information may be found in the online version of this article at the publisher's web-site:

http://dx.doi.org/10.1111/bph.13022

Figure S1 AnxA6 alters cholesterol levels and distribution in A431 and MEF cells.
Figure S2 AnxA6 modulates actin cytoskeleton distribution in A431 and MEF cells.
Figure S3 Lck10-EGFP and Src15-mCherry distribution in DRMs and bulk membranes after subcellular fractionation of A431 and MEF ± AnxA6 cells.
Figure S4 Cluster analysis of Lck10-PS-CFP2 and Src15-PS-CFP2 in mβCD and LatB-treated A431 and MEF cells.